Original Article

JCBFM

Journal of Cerebral Blood Flow & Metabolism
2019, Vol. 39(3) 547–561

DOI: 10.1177/0271678X18815791
journals.sagepub.com/home/jcbfm
SAGE

Overexpression of LH3 reduces the incidence of hypertensive intracerebral hemorrhage in mice

Hao Li*, Haochen Xu*, Hongyan Wen, Tianlong Liu, Yingying Sun, Ning Xiao, Congxia Bai, Jing Ge, Xuliang Wang, Li Song, Yan Song, Yinhui Zhang and Jingzhou Chen

Abstract

Hypertensive intracerebral hemorrhage (ICH) is a devastating cerebrovascular disease with no effective treatment. Lysyl hydroxylase 3 (LH3) is essential for collagen IV intermolecular crosslinking and stabilization. Deficiency in LH3 affects the assembly and secretion of collagen IV and basement membrane (BM) integrity of vessels. Here, we investigated whether LH3 has significant implications for disease progression and therapeutic intervention. Spontaneous hypertensive ICH of mice was induced by angiotensin II and L-NAME treatment. The adeno-associated virus was delivered into brain by stereotactic injection to knockdown or overexpress LH3. We found LH3 levels were reduced in human patients with ICH and gradually decreased in mice before ICH. LH3 knockdown increased the incidence of hypertensive ICH in mice. The incidence, number, and size of ICHs in mice were markedly reduced by LH3 overexpression. RNA-seq revealed that LH3 overexpression significantly reversed the profound alterations in gene transcriptional profiles of cerebral vessels. LH3 overexpression was sufficient to enhance BM integrity, inhibit matrix metalloproteinase activity, attenuate microglial activation and leukocyte infiltration, and reduce VSMC apoptosis before ICH. These results indicate that LH3 overexpression attenuates susceptibility to hypertensive ICH. We emphasize that LH3 modulation may serve as a viable approach for future investigations of ICH prevention.

Keywords

Basement membrane, hypertension, intracerebral hemorrhage, LH3, transcriptome

Received 11 May 2018; Revised 16 October 2018; Accepted 16 October 2018

Introduction

Spontaneous intracerebral hemorrhage (ICH) is a devastating form of cerebrovascular disease with particularly high mortality and disability rates,[1,2] and chronic hypertension is a major risk factor for ICH.[3] The majority of investigations have been focused on the pathophysiology and potential therapeutic strategies of subsequent brain injury after ICH. However, the precise mechanisms that contribute to the pathogenesis of ICH remain poorly understood, and therefore few effective treatments are available for prevention.[4]

Collagen IV, which is a crucial extracellular matrix (ECM) molecule and the main component of the basement membrane (BM), forms a network that is integral to the structure of cerebral vessels. Accumulating evidence has shown that mutations in the genes that encode collagen IV alpha 1 (COL4A1) and alpha 2 (COL4A2) cause disruptions in the BM and highly spontaneous ICHs in human and mouse models.[5–7] Lysyl hydroxylase (LH) is an enzyme that catalyzes the hydroxylation of lysine residues in collagens and other proteins with collagen-like sequences. In particular, LH3 (encoded by *PLOD3*), but not LH1 or LH2, is

State Key Laboratory of Cardiovascular Disease, Fuwai Hospital, National Center for Cardiovascular Diseases, Chinese Academy of Medical Sciences and Peking Union Medical College, Beijing, China

*These authors contributed equally to this work.

Corresponding author:
Jingzhou Chen, State Key Laboratory of Cardiovascular Disease, Fuwai Hospital, National Center for Cardiovascular Diseases, Chinese Academy of Medical Sciences and Peking Union Medical College, 167 Beilishi Road, Xicheng District, Beijing 100037, China.
Email: chendragon1976@aliyun.com

the only isoenzyme that generates hydroxylysine-linked carbohydrates because of its glucosyl galactosyltransferase (GGT) activities, which are indispensable for collagen IV intermolecular crosslinking and the stabilization of collagen structure.[8] Notably, recent studies have demonstrated that a deficiency in LH3 affects the assembly and secretion of collagen IV and BM stability.[9] Mutations in the LH3 gene cause embryonic lethality with the premature aggregation of collagen IV in mice.[10] However, whether there is a causal or direct participatory role for LH3 deficiency in the development of ICH remains unknown.

Therefore, the aim of this study was to determine whether LH3 was decreased in ICH and whether a gain of LH3 had potential therapeutic value for reducing the incidence of hypertensive ICH. In this study, we examined LH3 levels in ICH patients and observed dynamic changes in a mouse model of spontaneous ICH induced by hypertension. More importantly, we assessed the effects of LH3 knockdown or overexpression on the incidence, number, and size of ICHs in mice. Furthermore, alterations in the gene transcriptional profile that were revealed by RNA-seq unmasked the underlying mechanisms of LH3 in its protective effect against ICH.

Materials and methods

Human blood sample collection

The study protocol was reviewed and approved by the Human Ethics Committee, Fuwai Hospital (Approval No.: 2016-732), and the study was conducted in accordance with the principles of Good Clinical Practice and the Declaration of Helsinki. Written informed consent was obtained from all study participants or their legal proxies. ICH patients were recruited simultaneously from the same demographic area through June 2017 to October 2017 from Cangzhou Central Hospital. We included 34 ICH patients who had noncontract computed tomographic brain scans or magnetic resonance imaging (MRI) brain scans. Patients with other types of hemorrhagic stroke (i.e. subarachnoid hemorrhage, intracranial aneurysm, or cerebrovascular malformation) or severe systemic diseases (collagenosis, endocrine, inflammation, liver neoplastic, or renal diseases) were excluded. Thirty-four controls were selected from community-based inhabitants free of a history of stroke and neurological diseases following the same exclusion criteria as the ICH patients. Controls were matched to ICH patients for sex and age.

Baseline data, including demographic characteristics, body mass index, systolic blood pressure, diastolic blood pressure, blood glucose, total plasma cholesterol (TC), triglycerides (TGs) and cigarette smoking were collected. Hematoma volume was measured using the ABC/2 method as previously described,[11,12] where A is the greatest hemorrhage diameter by CT or MRI, B is the diameter 90° to A, and C is the approximate number of slices with hemorrhage multiplied by the slice thickness.

Experimental animals

Animal experiments were approved by the Committee of Fuwai Hospital on Ethics of Animal Experiments (Approval No.: 0085-M-200-HX) and complied with the National Institutes of Health's Guide for the Care and Use of Laboratory Animals, and the manuscript adheres to the ARRIVE (Animal Research: Reporting of In Vivo Experiments) guidelines for reporting animal experiments. Male wild-type C57BL/6N mice, eight months old (28–34 g), were purchased from the National Resource Center of Model Mice (NRCMM). Female mice were not used to avoid any influence of sex steroids. A total of 288 mice were used. All mice were housed in a specific pathogen-free environment under a 12 h/12-h light-dark cycle and fed rodent diet *ad libitum*. All animal surgeries were performed under anesthesia. Animals were randomly assigned to experimental groups by using the random number generator function in SPSS.[13] Investigators blinded to the treatment groups evaluated outcomes in all mice and performed the analysis.

There were three cohorts of mice in this study (Supplemental Figure 1). The first and second cohorts were used to evaluate blood pressure and the incidence and size of ICH. Mice in these cohorts were euthanized with an injection of Nembutal (150 mg/kg, intraperitoneal, i.p., Sigma-Aldrich, MO, USA) when a mouse developed signs of stroke or on day 28 after pump implantation if the mouse did not have neurologic signs. When a mouse developed signs of stroke, it and a second mouse without neurologic signs from the vehicle group were euthanized to collect tissue samples after the same duration of treatment. The third cohort was used to perform RNA sequencing of brain microvessels, validate the expression of mRNA and evaluate vasculopathy before the mice developed any neurologic signs.

Construction and stereotactic injection of vectors for LH3 knockdown and overexpression

For local knockdown of LH3 in vivo, recombinant adeno-associated virus (AAV) serotype 9 vector expressing a short hairpin RNA (shRNA) directed at LH3 (AAV-shLH3) or a control hairpin (AAV-shCON) was used (GeneChem, Shanghai, China). The shRNA expression was driven by a mouse U6 promoter (pol III) and used GFP as a reporter. The final virus in

phosphate-buffered saline (PBS) had a titer of 3×10^{12} viral particles/ml. To induce exogenous expression of LH3 in vivo, we constructed a pAAV9-LH3-p2A-GFP vector (AAV-LH3) by inserting mouse LH3 cDNA into pAAV9-p2A-GFP between two ITRs (ViGene Biosciences, Shandong, China). AAV carrying GFP (AAV-GFP) was simultaneously prepared as a control vector. A detailed experimental description can be found in the online supplementary material.

Animal model of spontaneous ICH

The methods used to produce spontaneous ICH and to assess signs of experimental stroke are described elsewhere.[14] Briefly, mice were treated with angiotensin II (AngII; 1000 ng/kg per min; Sigma-Aldrich, MO, USA) via osmotic pumps (Durect Corporation, CA, USA) that were implanted subcutaneously (s.c.) in mice under anesthesia with 2% isoflurane in an O_2 mixture (1 L/min). Treatment with L-NAME (100 mg/kg per day; Sigma-Aldrich, MO, USA) in drinking water was started on the same day as the implantation of osmotic pumps. After one week, transient acute hypertension was induced by daily AngII injections (0.5 mg/g, s.c., twice daily from day 7 to day 28 after pump implantation). Vehicle groups of mice had a saline-filled osmotic pump implanted and received saline injections at the same time points. Sham groups of mice received only sham operation with no pump implanted. Systolic blood pressure was measured in conscious mice on day 7 after pump implantation using tail-cuff plethysmography (BP-2010A, Softron, Japan).

Clinical signs of stroke including circling behavior, contralateral forelimb extension, and other motor dysfunction were assessed by daily neurological examinations three times per day as previously described.[15] After the appearance of stroke symptoms, mice were transcardially perfused with ice-cold PBS, and the brains were collected for further experiments.

ICH assessment by MRI

MRI was performed on a dedicated 7T MR Varian horizontal bore MRI system (183-mm horizontal bore; Varian, Palo Alto, CA).[16,17] Briefly, mice were anesthetized with 2% isoflurane in an O_2 mixture (1 L/min). The imaging protocol for all of the mice included T2* gradient-echo sequences (repetition time/echo time = 250/5 ms). The field of view was 20×20 mm, and the matrix was 256×256 mm. Twelve coronal slices were acquired from the frontal pole to the brain stem, and the images were preserved as 256×256-pixel images. The T2* lesion was outlined along the border of the hyperintense area, and the lesion volume was obtained by combining the hyperintense area over all slices and multiplied by sections thickness.

Isolation of cerebral vessels

Brains were collected for the isolation of cerebral vessels as previously described.[18,19] During this period, mice did not develop any neurologic signs. Briefly, mice were transcardially perfused with ice-cold PBS. Then, the brains were removed, rinsed in cold isotonic sucrose buffer (0.32 mol/L sucrose, 3 mmol/L HEPES, pH 7.4), and cleared of pia mater and choroid plexus. The brain was homogenized with a tight-fitting pestle Dounce homogenizer in 5 ml of sucrose buffer. The homogenate was centrifuged at 1000*g* for 10 min. A detailed experimental description can be found in the online supplementary material.

Tissue preparation and hematoxylin–eosin staining

Brains were immersed in 4% paraformaldehyde for 6 h at 4°C and then cryoprotected in 20% sucrose at 4°C overnight. Frozen coronal sections were cut at 20-μm thickness. For hematoxylin–eosin (H&E) staining, sections were incubated in hematoxylin for 2 min and eosin for 1 min. The wall thickness of the cerebral artery was quantified after H&E staining by using ImageJ software.[20]

Quantification of hemorrhages

Histological analysis of brain hemorrhages was performed using H&E staining as previously described.[21] Briefly, one of every five serial sections was used for the determination of the size and number of ICHs across the entire brain.[15] The ICH images were acquired by Leica DM6000B microscope. The number of hemorrhages $>10^{-6}$ mm^3 in the area was quantified using ImageJ software. The size of hemorrhages was estimated as follows: (area (mm^2) of ICHs in each section) $\times$ (20×10^3 (mm): distance between successive sections).[22] For the quantification of hemorrhages, Drabkin reagent (500 μl, Sigma-Aldrich, MO, USA) was added to the hemispheric brain tissue of each mouse, followed by homogenization and centrifugation at 13,000 r/min for 30 min. The optical density of the supernatant was measured by spectrophotometry (Thermo Fisher Scientific, IL, USA) at 540 nm. Hemorrhage volume was expressed in equivalent units by comparison with a reference curve as previously described.[23]

TUNEL staining

TUNEL (terminal deoxynucleotidyl transferase-mediated dUTP nick-end labeling, Sigma-Aldrich,

MO, USA) was evaluated using an in situ cell death detection kit. Briefly, sections were incubated with alpha-SMA and secondary antibodies, followed by incubation with TUNEL mix according to the manufacturer's instructions. We assessed the numbers of $TUNEL^+$ cells in α-SMA^+ arteries by using ImageJ software.[24]

Immunohistochemistry

The frozen sections were immunostained using a previously described protocol.[21] The following primary antibodies were used: goat anti-CD31 (AF3628, R&D Systems Incorporated, MN, USA), rabbit anti-Plod3 (LH3) (ab128698, Abcam, MA, USA), anti-actin, α-smooth muscle-Cy3™ antibody (αSMA, clone 1A4, C6198, Sigma-Aldrich, USA), rabbit anti-collagen IV (ab19808, Abcam, MA, USA), goat anti-Iba-1 (ab5076, Abcam, MA, USA), rat anti-Ly6G (551459, BD Pharmingen, USA), anti-F4/80 (ab6640, Abcam, MA, USA), rabbit anti-NeuN (ab177487, Abcam, MA, USA), and mouse anti-CC1 (OP80, Millipore, MA, USA). The following secondary antibodies were used: Alexa Fluor 594-conjugated donkey anti-goat IgG, Alexa Fluor 594-conjugated donkey anti-rat IgG, Alexa Fluor 488-conjugated donkey anti-rat IgG, Alexa Fluor 488-conjugated donkey anti-rabbit IgG, Alexa Fluor 488-conjugated donkey anti-mouse IgG, and Alexa Fluor 488-conjugated donkey anti-mouse IgG (all from Abcam, MA, USA). All of the images were visualized by Leica SP8 laser-scanning confocal microscope and Leica DM6000B microscope. Images indicating the successful transfection of AAV were obtained with a Panoramic Confocal Scanner (3DHISTECH, Budapest, Hungary) using 1.20 Sp1 scanner software. The criteria for the identification of activated microglia were a combination of morphology and a cell body diameter cutoff of 7.5 μm for the $Iba\text{-}1^+$ cells.[25] Collagen IV coverage was determined as the percentage of collagen IV^+ area covering the $CD31^+$ area in 0.078-mm^2 regions. For the quantification of all markers, four random fields from three sections (with coordinates 1.2 mm, 2.2 mm and 3.2 mm posterior to a bregma) were captured using a 40 × objective. Six mice per group were examined.

Western blot detection of LH3 in cerebral vessels

Cerebral vessel samples were lysed/homogenized in lysis buffer for 15 min at 4°C and then centrifuged at 12,000*g*. The resulting supernatants were subjected to sodium dodecyl sulfate–polyacrylamide gel electrophoresis (SDS–PAGE) and blotted onto nitrocellulose membranes. The membranes were then incubated with antibodies directed against LH3 (11027-1-AP, Proteintech, IL, USA), and the protein bands were visualized with SuperSignal West Dura Extended Duration Substrate (Thermo Fisher Scientific, IL, USA). The blots were subsequently probed with GAPDH (ab8245, Abcam, MA, USA) to confirm equal loading.

Gelatin zymography

Zymography was performed as previously described.[26,27] Briefly, equal amounts of protein from the cerebral vessel samples were loaded and separated on a 10% Tris-glycine gel with 0.1% gelatin as the substrate. Then, the gel was washed and renatured with 2.5% Triton X-100 buffer. After incubation with developing buffer at 37°C for 24 h, the gel was stained with 0.05% Coomassie R-250 dye (Sigma-Aldrich, MO, USA) for 30 min and destained. Gelatinase standard was mixed with pro-MMP-9 and pro-MMP-2 (Sino Biological Incorporated, Beijing, China). Pro-MMP-9 activity was evaluated by optical density and normalized to that of the vehicle group.

Total RNA isolation

Total RNA from the cerebral vessel samples was extracted using the RNeasy Mini Kit with on-column DNase step (Qiagen, Hilden, Germany) according to the manufacturer's protocol. Immediately following extraction, the total RNA concentration and A260:A280 ratio of each sample were determined via NanoDrop 2000 (Thermo Fisher Scientific, IL, USA).

RNA sequencing

Total RNA was purified by using an RNeasy micro kit (QIAGEN, Hilden, Germany). The TruSeq RNA Sample Preparation Kit V2 (Illumina, San Diego, CA) was used for next-generation sequencing library construction per the manufacturer's protocol. The sequencing was performed by Shanghai Biotechnology Corporation (Shanghai, China) using the Illumina high-throughput HiSeq 2500 platform. A detailed experimental description can be found in the online supplementary material.

Quantitative real-time PCR

Relative quantification by real-time PCR was performed using SYBR Green to detect PCR products in real time with the ABI PRISM 7500 Sequence Detection System (Applied Biosystems). Melting curve analysis was performed at the end of each PCR reaction. The sequences of oligonucleotide primers were designed according to the cDNA sequences in the GenBank database using Primer Express software

(Applied Biosystems) and are listed in Supplemental Table 1.

ELISA

The plasma levels of LH3 were measured for ICH patients and controls using ELISA kit (Abbexa, Cambridge, UK). The LH3 levels of mice from cerebral vessels and plasma were measured using ELISA kit (LMAI Bio, Shanghai, China). The plasma levels of IL-6 and TNF-α in mice were measured using ELISA kits (R&D Systems Incorporated, MN, USA). All values were in the linear range and were calculated based on known protein concentrations.

Statistics

Data are expressed as the mean $\pm$ SD. For parametric data, Student's *t*-test or ANOVA was used to analyze the differences among groups if the data were determined to follow a normal distribution. For nonparametric data, the Mann–Whitney U test was used to analyze the differences between two groups. A Kruskal–Wallis ANOVA combined with Dunn's post hoc multiple comparison test was performed when more than two groups were evaluated. Statistical comparisons of percentages were performed using χ^2 analysis. Correlations were determined with the Pearson correlation test. The cumulative incidence of the signs of stroke was evaluated using a log-rank test. Data were analyzed using GraphPad Prism (GraphPad Software Inc., CA, USA). $P < 0.05$ was considered statistically significant.

Results

LH3 levels are decreased in the plasma of patients and cerebral vessels of mice with ICH

To investigate whether LH3 levels are decreased in human patients with ICH, the plasma samples of 34 ICH patients and controls were collected. The baseline characteristics are shown in Supplemental Table 2. Patients with ICH showed lower plasma LH3 levels (Figure 1(a)). Detailed hemorrhagic information of the patients, including ICH volume, hematoma location and the time point of blood collection, is shown in Supplemental Table 3. Similarly, LH3 levels of plasma were also decreased in a mouse model of spontaneous ICH which was induced by AngII and L-NAME treatment (Supplemental Figure 2(a)). To investigate whether LH3 levels in cerebral vessels were altered in a similar manner compared with blood samples, we next isolated the cerebral vessels of mice (Supplemental Figure 2(b)) and explored the dynamic changes in LH3 upon AngII and L-NAME treatment at various time points. As shown in Figure 1(b), reduced LH3 mRNA levels were detected on day 3, and further reductions were observed on day 5 and when mice developed ICH. Because LH has three isoforms (LH1, LH2, and LH3) with different degrees of LH activity characterized in various tissues, we also examined the mRNA levels of the LH1 and LH2 isoenzymes in mice with ICH. Although LH1 was also reduced in cerebral vessels, the extent of the reduction was less than that of LH3, while the level of LH2 remained unchanged (Supplemental Figure 2(c)). The reduced protein levels of LH3 in the cerebral vessels were validated by Western blot analysis and ELISA when mice developed ICH (Figure 1(c), Supplemental Figure 2(d)). Furthermore, correlation analysis indicated that plasma LH3 levels positively correlated with LH3 levels of cerebral vessels in mice with ICH (Supplemental Figure 2(e)). Using immunofluorescence staining, we found that LH3 was predominantly detected in $CD31^+$ cerebral vessels of the brain. The expression of LH3 was also found in neurons and oligodendrocytes (identified by the $NeuN^+$ and $CC1^+$ markers, respectively) (Supplemental Figure 3). Importantly, the $LH3^+$ fluorescence intensity including that in cerebral vessels was significantly decreased after ICH. Moreover, neither the expression of LH3 in brain nor the percent area occupied by $CD31^+$ vascular structures was significantly different between the sham group and the vehicle group (Figure 1(c) and (d), Supplemental Figure 3, Supplemental Figure 4). Hence, we did not include the sham group in further experiments in the present study. Taken together, our data reveal that levels of LH3 are gradually decreased in cerebral vessels during the progression of hypertensive cerebral hemorrhage.

LH3 knockdown exacerbates hypertension-induced spontaneous ICH

To more directly determine whether there is a causal relationship between LH3 and spontaneous ICH, AAV-shRNA-treated mice (Supplemental Figure 5(a)) were subjected to chronic AngII perfusion and concomitant L-NAME treatment. Additionally, mice received a daily AngII bolus starting on day 7 after pump implantation. We first validated the viral vector strategy by measuring LH3 expression with Western blotting and immunohistochemistry. Protein levels of LH3 were significantly downregulated in cerebral vessels two weeks after AAV-shLH3 delivery relative to the levels in the AAV-shCON group. Immunofluorescence staining also revealed clearly decreased LH3 levels in cerebral vessels and perivascular areas (Supplemental Figure 5(b) and (c)). These data

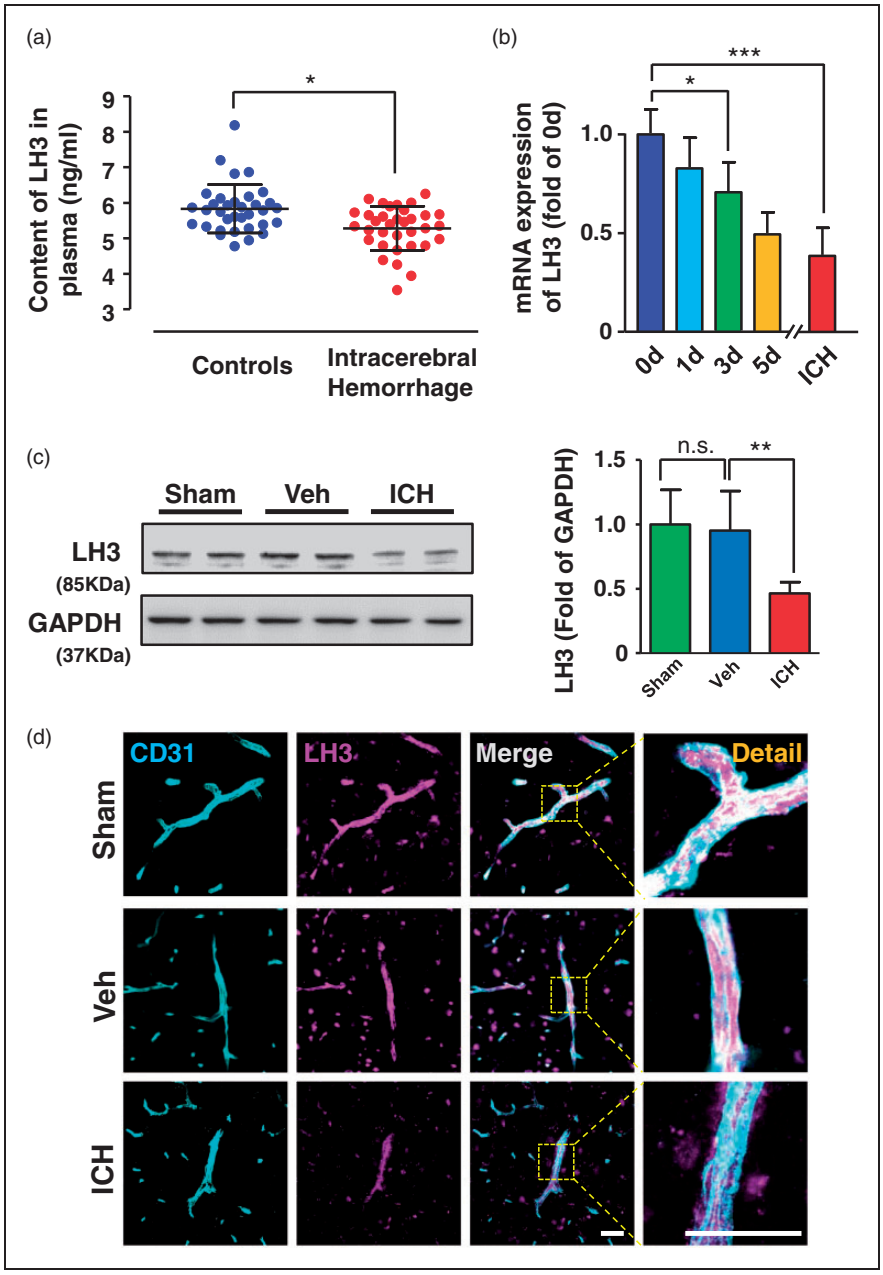

Figure 1. LH3 levels are decreased in the plasma of patients and cerebral vessels of mice with intracerebral hemorrhage (ICH). (a). The concentrations of LH3 in human patients with ICH and in controls were measured by ELISA. $n = 34$. $^{*}P < 0.05$; Student's unpaired two-tailed *t*-test. (b). Quantitative PCR was used to evaluate the level of LH3 in the cerebral vessels of mice at different time points after pump implantation. $n = 5$–6. $^{*}P < 0.05$, $^{***}P < 0.001$; one-way ANOVA with Bonferroni post hoc test at each time point. (c). Western blot analysis of LH3 in the cerebral vessels of the sham, vehicle (Veh) and ICH groups when mice developed ICH. $n = 6$. $^{*}P < 0.01$, n.s. indicates not significant; one-way ANOVA with Bonferroni post hoc test. (d). Representative images of LH3 expression in $CD31^{+}$ cerebral vessels in the mice of each group when mice developed ICH. Bar = 50 μm. Data are the mean±SD.

suggest that AAV-shLH3 mediates the successful knockdown of LH3 in vivo. During the experimental period, 70% of the AAV-shCON-treated mice showed signs of clinical manifestation of ICH. In contrast, 90% of mice in the AAV-shLH3 group developed signs of ICH, which occurred within a similar time window (Figure 2(a)). Furthermore, we performed T2*-weighted MRI to manually delineate and measure hematoma lesion volume, which showed an apparent relative increase in AAV-shLH3-treated brains (Figure 2(b)). Histological analysis confirmed that the AAV-shLH3-treated mice had increased hemorrhage

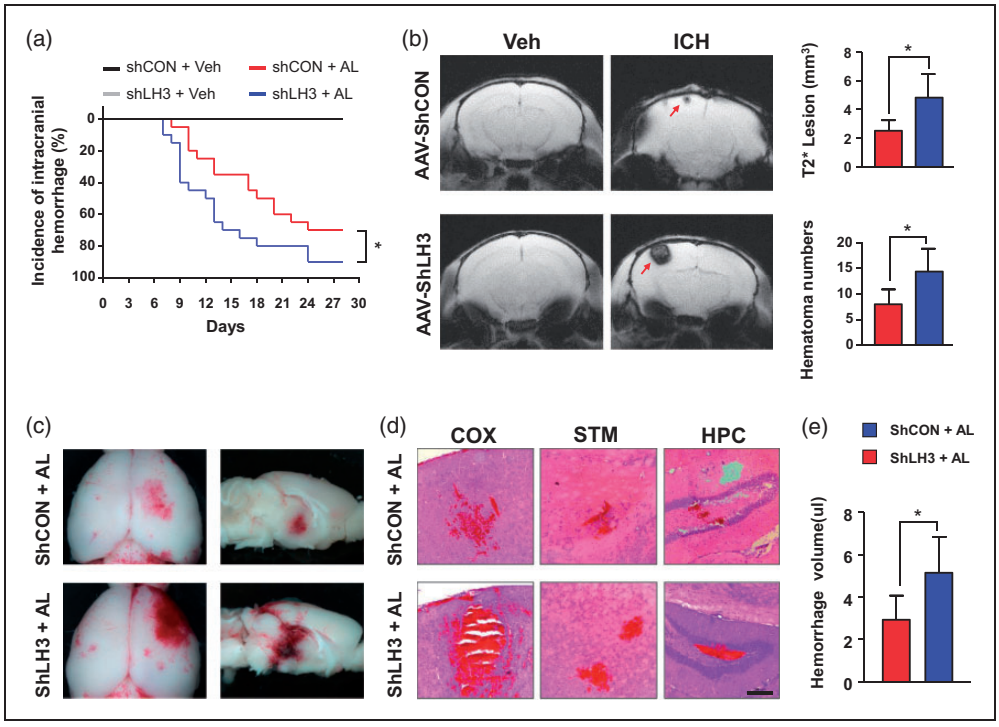

Figure 2. LH3 knockdown exacerbates hypertension-induced spontaneous intracerebral hemorrhage (ICH). (a). Kaplan–Meier plot of the signs of stroke in each group. $n = 20$. *$P < 0.05$; Log-rank (Mantel–Cox) test. (b). MRI scans with T2* gradient-echo sequences were performed to assess lesion size and number when mice developed signs of stroke. $n = 6$. *$P < 0.05$; Student's unpaired two-tailed *t*-test. (c). Representative images of the dorsal surface and a sagittal section of the brain showing ICH in each group. (d). Representative images of cerebral hemorrhage in cortex (COX), striatum (STM), and hippocampus (HPC) sections stained with hematoxylin and eosin (H&E) (bar = 200 μm). (e). Quantification of intracerebral hemorrhage by spectrophotometric hemoglobin assay. $n = 6$. *$P < 0.05$; Student's unpaired two-tailed *t*-test. Arrows indicate hemorrhages. AL: AngII plus L-NAME; Veh: vehicle. Data are the mean±SD.

numbers and size in the brain relative to the number and size in AAV-shCON-treated mice (especially in the cortex, striatum, and hippocampus) (Figure 2(c) and (d), Supplemental Figure 5(d)). By using a spectrophotometric hemoglobin assay, we found that LH3 knockdown resulted in a significant increase in hemorrhage volume (Figure 2(e)). Taken together, these data demonstrate that LH3 deficiency exacerbates hypertension-induced spontaneous ICH.

Overexpression of LH3 reduces susceptibility to hypertension-induced spontaneous ICH

To explore the possible role of LH3 in maintaining the integrity and homeostasis of cerebral vessels and the potential for LH3 as a target for the prevention of ICH, we constructed an AAV-LH3 vector to induce the exogenous expression of LH3 in vivo (Supplemental Figure 6(a)). Green fluorescence was detectable in brain sections four weeks after delivery, indicating the successful transfection of AAV (Supplemental Figure 6(b)). Furthermore, lower-magnification images acquired by a whole-slide imaging system demonstrated that green fluorescence was present in peri-intraventricular areas as well as the brain parenchyma, especially in the cortex (Supplemental Figure 6(c)). Furthermore, the mRNA and protein levels of LH3 were significantly upregulated in cerebral vessels of the AAV-LH3 group four weeks after delivery relative to the levels in the AAV-GFP group (Supplemental Figure 6(d) and (e)). Immunofluorescence staining revealed significantly increased LH3 accumulation in cerebral vessels and perivascular areas (Supplemental Figure 6(f)).

Furthermore, AAV-treated mice were subjected to the model of ICH. Blood pressure was significantly increased in the AAV-GFP group, and AAV-LH3 treatment did not further affect blood pressure (Supplemental Figure 7). Seventy-five percent of mice in the AAV-GFP group showed signs of ICH. In contrast, 30% of mice in the AAV-LH3-treated group developed signs of ICH after LH3 overexpression, and this incidence was significantly lower than that in the AAV-GFP group (Figure 3(a)). Furthermore, T2*-weighted MRI showed an apparent decrease in lesion size and numbers in the AAV-LH3-treated

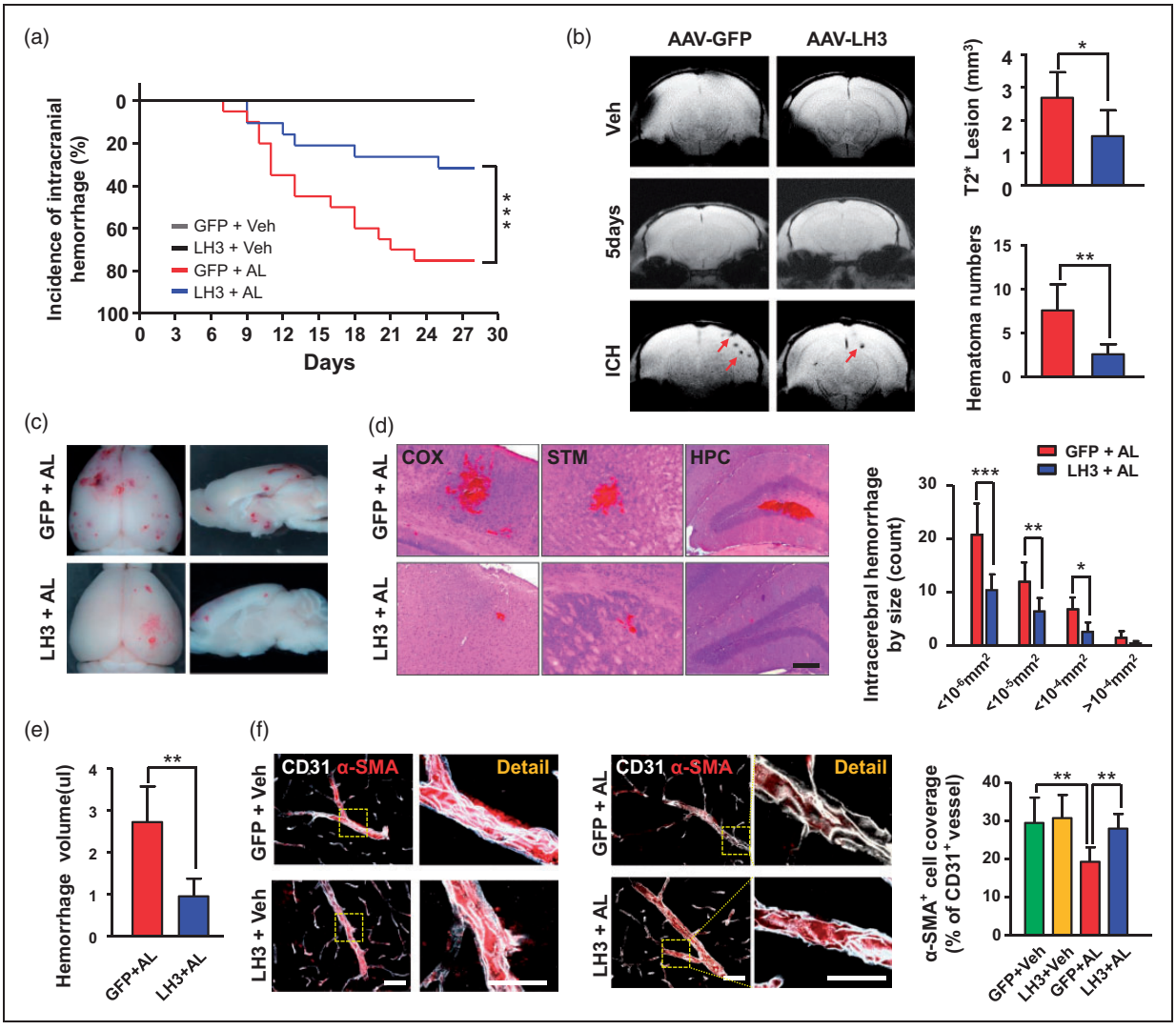

Figure 3. Overexpression of LH3 reduces susceptibility to hypertension-induced spontaneous intracerebral hemorrhage (ICH). (a). Kaplan–Meier plot of the signs of stroke in each group. $n = 20$. ***$P < 0.001$; Log-rank (Mantel–Cox) test. (b). MRI scans with T2* gradient-echo sequences were performed to assess lesion size and number on day 5 after pump implantation and when mice developed signs of stroke. $n = 6$. *$P < 0.05$, **$P < 0.01$; Student's unpaired two-tailed *t*-test. (c). Representative images of the dorsal surface and a sagittal section of the brain show ICH in each group. (d). Left: Representative images of cerebral hemorrhage in cortex (COX), striatum (STM), and hippocampus (HPC) sections stained with hematoxylin and eosin (H&E) (bar = 200 μm). Right: Quantification of the distribution of ICH by size in GFP+AL mice (n = 15) and LH3+AL mice (n = 6). *$P < 0.05$, **$P < 0.01$, ***$P < 0.001$; Student's unpaired two-tailed *t*-test or the Mann–Whitney U test. (e). Quantification of intracerebral hemorrhage by spectrophotometric hemoglobin assay. $n = 6$. **$P < 0.01$; Student's unpaired two-tailed *t*-test. (f). Representative images and quantification of α-SMA$^+$ vascular smooth muscle cell coverage on the CD31$^+$ cerebral vessels of each group. (Bar represents 50 μm in merged images and 25 μm in enlarged images.) $n = 6$. **$P < 0.01$; two-way ANOVA with Bonferroni post hoc test. Arrows indicate hemorrhages. AL: AngII plus L-NAME; Veh: vehicle. Data are the mean±SD.

group (Figure 3(b)). Histological analysis confirmed that the AAV-LH3-treated mice had decreased hemorrhage size and numbers in the brain (Figure 3(c) and (d)). We also confirmed that LH3 overexpression resulted in a significant decrease in hemorrhage volume by spectrophotometric hemoglobin assay (Figure 3(e)). Because vascular smooth muscle cells (VSMCs) play a crucial role in maintaining the integrity and function of small arteries and arterioles, we used a VSMC-specific marker, namely, smooth muscle α-actin (α-SMA), to investigate the pathological changes in vessels that were responsible for

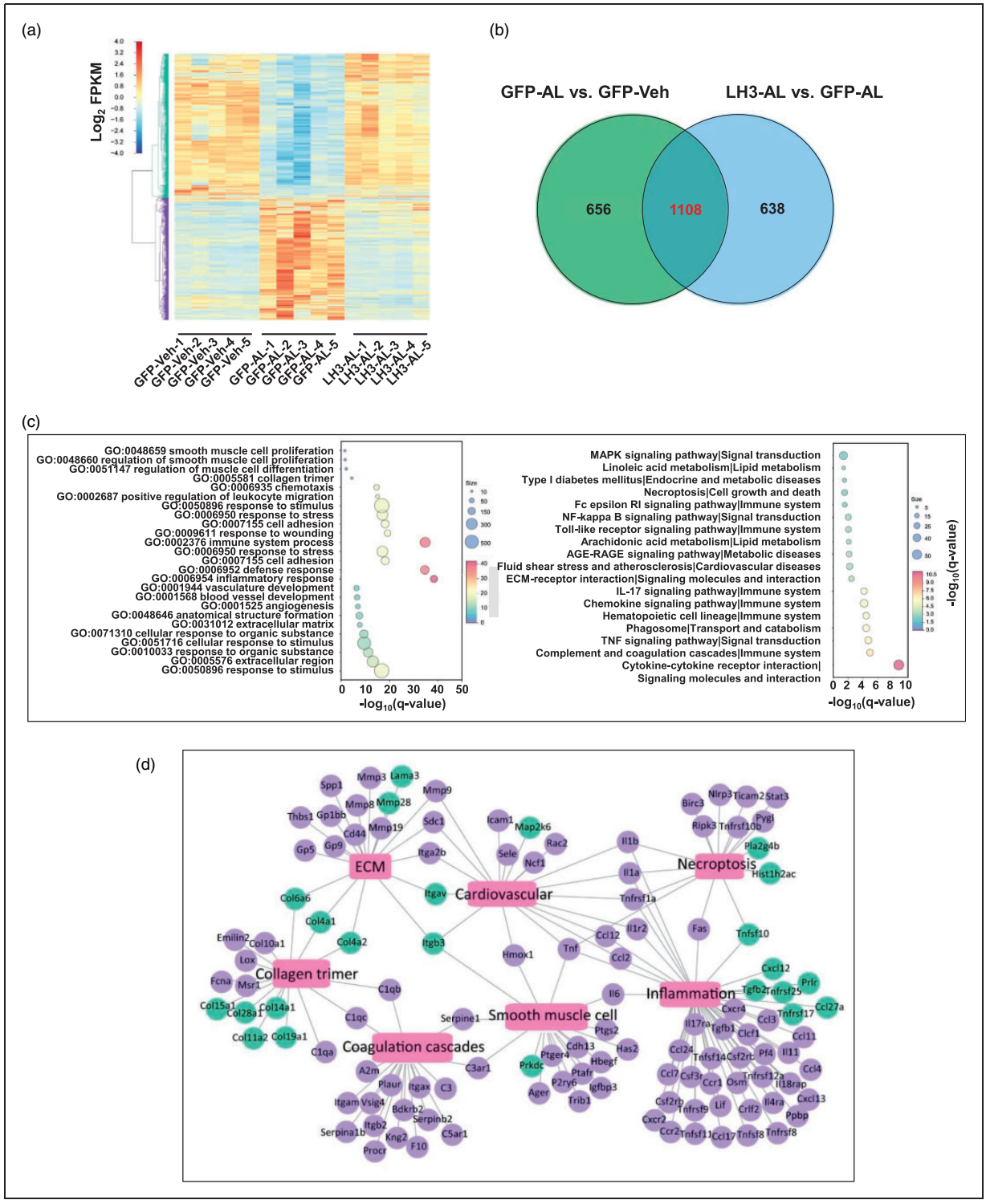

Figure 4. LH3 overexpression reverses the profound alterations in the hypertension-induced gene transcriptional profile of cerebral vessels. (a). Heat map of cluster analysis shows the transcript expression levels of differentially expressed genes (DEGs) in the cerebral vessels of the AAV-GFP and AAV-LH3 groups on day 5 after AngII plus L-NAME (AL) or vehicle (Veh) treatment. The color scale illustrates the relative expression levels across all samples: red represents an expression level above the mean, and blue represents an expression level lower than the mean. The dendrogram on the left of the heat map shows the clustering of the transcripts. (b). Venn diagram shows the number of DEGs. Numbers in the green cycle represent the DEGs between the AL group and the Veh group after AAV-GFP treatment. Numbers in the purple cycle represent the DEGs in the AL group after AAV-LH3 treatment. (c). Top terms showing enrichment based on $-\log_{10}$(q-value) from gene ontology (GO) enrichment analysis (Left) and KEGG pathway analysis (Right) of the DEGs significantly reversed by AAV-LH3 treatment. (d). Network of significantly enriched GO and KEGG pathway terms for DEGs significantly reversed by AAV-LH3 treatment. The blue nodes denote DEGs upregulated by AAV-LH3 treatment, and the purple nodes denote DEGs downregulated by AAV-LH3 treatment. Pink rectangles represent significantly enriched terms. $n = 5$ per group.

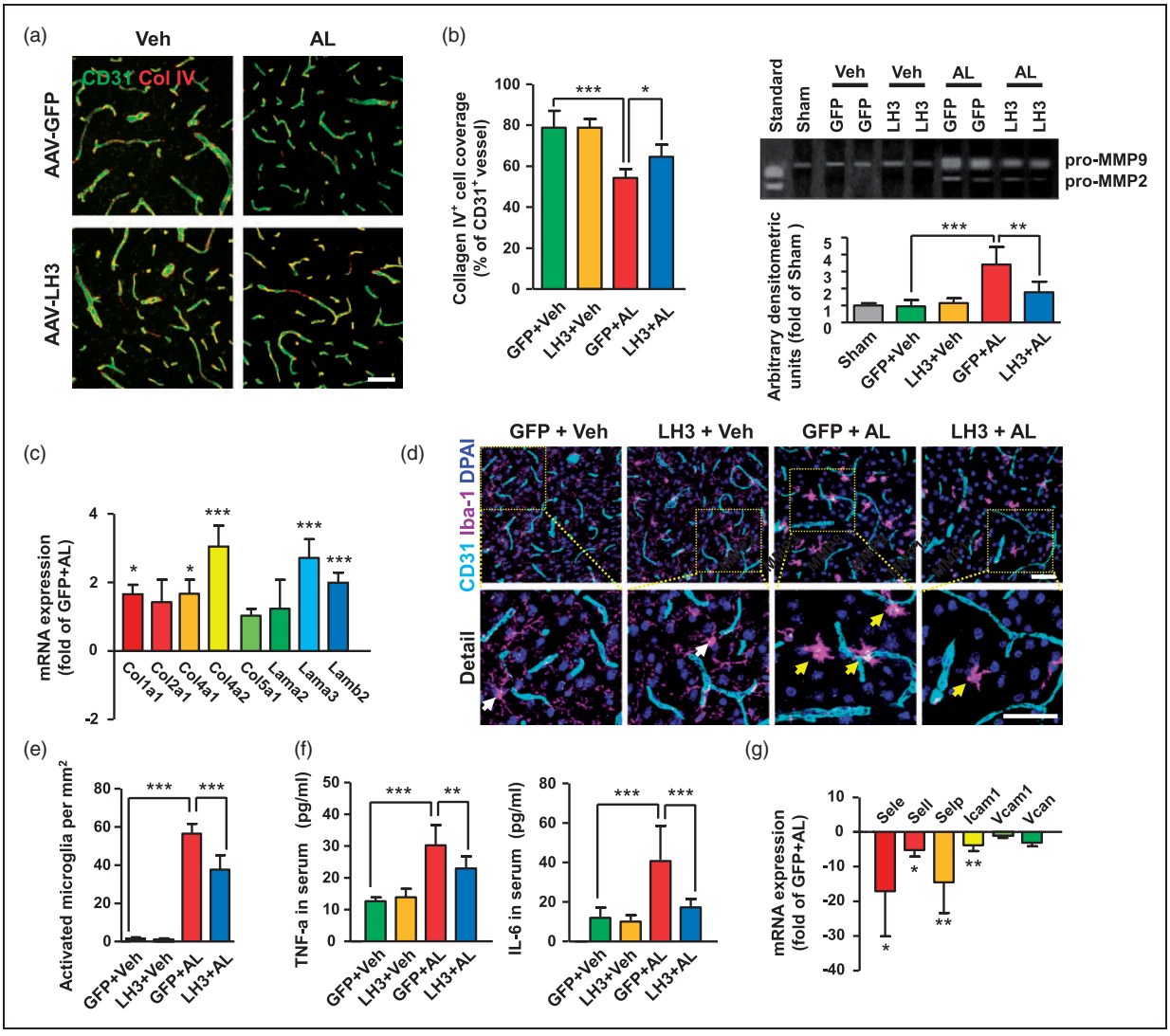

Figure 5. Extracellular matrix remodeling and inflammatory processes can be ameliorated by LH3 overexpression. (a). Representative images and quantification of collagen IV (Col IV) basement membrane (BM) coverage on the CD31$^+$ cerebral vessels of each group five days after AngII plus L-NAME (AL) or vehicle (Veh) treatment. $n = 6$. $^*P < 0.05$, $^{***}P < 0.001$; two-way ANOVA with Bonferroni post hoc test. (b) Representative gelatin zymography and quantitative analysis of MMP-9 activity of cerebral vessels on day 5 after AL treatment. $n = 6$. $^{**}P < 0.01$, $^{***}P < 0.001$; one-way ANOVA with Bonferroni post hoc test. (c). Quantitative PCR (qPCR) was used to evaluate the expression of pivotal components of the BM in isolated cerebral vessels. $n = 6$. $^*P < 0.05$, $^{***}P < 0.001$; Student's unpaired two-tailed *t*-test. Representative images (d) of Iba-1$^+$ microglial immunostaining and the quantification (e) of activated microglia surrounding cerebral vessels. $n = 6$. $^{***}P < 0.001$; two-way ANOVA with Bonferroni post hoc test. (f). Levels of proinflammatory cytokines TNF-α (Left) and IL-6 (Right) in serum were measured by ELISA. $n = 6$. $^{**}P < 0.01$, $^{***}P < 0.001$; two-way ANOVA with Bonferroni post hoc test. (g). mRNA expression levels of cerebral artery adhesion molecules were evaluated by qPCR. $n = 6$. $^*P < 0.05$, $^{**}P < 0.01$; Student's unpaired two-tailed t-test. Bar represents 50 μm. Arrows indicate activated microglia. Data are the mean±SD.

hemorrhage. A dramatic decrease in the α-SMA coverage of arterioles from the ICH mice was observed, and the decrease was significantly reversed by AAV-LH3 intervention (Figure 3(f)). Thus, these data clearly demonstrate the essential roles of LH3 in reducing susceptibility to hypertension-induced spontaneous ICH.

LH3 overexpression reverses the profound alterations in the hypertension-induced gene transcriptional profile of cerebral vessels before ICH

To gain mechanistic insights into the protective effects of LH3 against ICH, a whole-transcriptomic analysis of cerebral vessels was performed using RNA-seq on day

5 after pump implantation. The sequencing data have been uploaded to the National Center for Biotechnology Information under GEO accession number GSE113151 and are publicly available. MRI was performed to validate the absence of ICH on day 5 (Figure 3(b)). A total of 1764 genes (863 upregulated and 901 downregulated) were differentially expressed (FDR<0.05) after AngII and L-NAME treatment relative to the vehicle group. After AAV-LH3 treatment, 1746 genes (830 downregulated and 916 upregulated) were differentially expressed compared with the expression observed in the AAV-GFP group (Figure 4(a), Supplemental Figure 8). Importantly, among the 1764 genes differentially expressed in the AAV-GFP group, 1108 (62.8%) were significantly reversed by the overexpression of LH3 (Figure 4(b)). Furthermore, the reversed gene list was subjected to GO enrichment analysis to identify the overrepresented biological functions and canonical pathways. The reversed genes belonged to multiple gene categories related to the immune system, inflammatory processes, smooth muscle cell proliferation and ECM remodeling, which are known potential mechanisms of ICH.[4] KEGG pathway analysis suggested that the genes modulated by LH3 were enriched in several important pathways, including inflammation-related pathways, such as the TNF and NF-kappa B signaling pathways (Figure 4(c)). The pivotal genes enriched in the top were signaling pathways were further validated by qPCR (Supplemental Figure 9). Additionally, to understand and visualize the global interactions of the genes reversed by AAV-LH3 treatment, overrepresentation analyses for biological processes and pathways were performed. The network representation of the enriched biological processes and pathways is shown in Figure 4(d). Taken together, the RNA-seq data reveal that LH3 overexpression reverses profound alterations in the gene transcriptional profile of cerebral vessels before ICH and that the protective mechanism mainly involves ECM modulation, smooth muscle cells and inflammation.

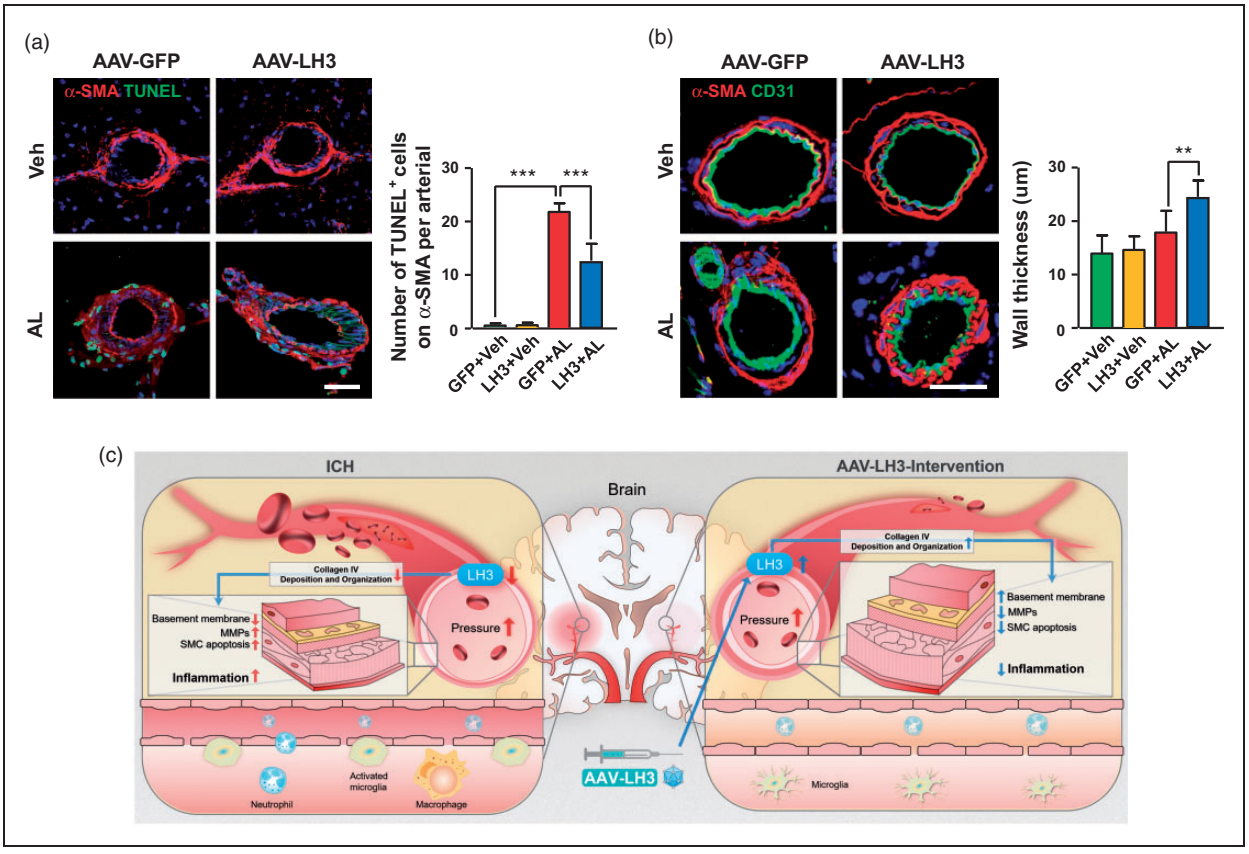

Figure 6. LH3 overexpression results in a significant decrease in vascular smooth muscle cell apoptosis. (a). Representative images and quantification of α-SMA$^+$ vascular smooth muscle cell apoptosis in each group five days after AngII plus L-NAME (AL) or vehicle (Veh) treatment. $n = 6$. ***$P < 0.001$; two-way ANOVA with Bonferroni post hoc test. (b). Representative images of α-SMA$^+$ vascular smooth muscle cells in mice. The wall thickness of cerebral small arteries in each group was quantified. $n = 6$. **$P < 0.01$; two-way ANOVA with Bonferroni post hoc test. (c). A working model of how LH3 reduces cerebral hemorrhage is shown. Bar = 50 μm. Data are the mean±SD.

ECM remodeling and inflammatory processes can be ameliorated by LH3 overexpression

LH3 is essential for the synthesis of collagen IV and, hence, for the stability of the BM. We observed that collagen IV coverage was significantly decreased on the cerebral vessels of AAV-GFP-treated mice, in which the LH3 levels were also markedly decreased on day 5 after pump implantation. Notably, collagen IV^+ BM coverage was 19% higher after AAV-LH3 treatment (Figure 5(a)). Matrix metalloproteinases (MMPs) in the vascular wall degrade collagen, laminin and other BM components, mediating ECM remodeling and compromising the structural integrity of the cerebral vasculature. Thus, we used gelatin zymography to assess MMP activity that was potentially important for ECM degradation. We found that MMP-9 activity was significantly reduced after AAV-LH3 treatment (Figure 5(b)). The mRNA levels of collagen I and laminin, which also play substantial roles in the composition of the vascular BM, were significantly increased after AAV-LH3 treatment (Figure 5(c)). Furthermore, the activation of microglia, as defined by morphologic criteria and an Iba-1^+ cell body diameter cutoff of 7.5 μm, was observed in the AAV-GFP group, indicating a critical impairment of BM structure and weakened microcirculation of cerebral vessels (Figure 5(d) and (e)). Moreover, the level of proinflammatory cytokine TNF-α, typically released by activated microglia, was markedly upregulated during hypertension (Figure 5(f)). Additionally, elevated mRNA expression levels of cerebral artery adhesion molecules and accumulated infiltration of macrophages and neutrophils in perivascular spaces were observed in the AAV-GFP group, suggesting triggered vascular inflammation (Figure 5(g), Supplemental Figure 10). Most importantly, both microglial activation and inflammatory processes were dramatically ameliorated by LH3 overexpression. Taken together, these data clearly demonstrate the essential roles of LH3 in maintaining the structural integrity of the BM and in blunting the inflammatory processes in cerebral vessels.

LH3 overexpression exhibits a significant decrease in the apoptosis of vascular smooth muscle cells

In cerebral small arteries and arterioles, VSMCs, mostly concentrated in the media, are the predominant matrix-synthesizing cells and provide structural integrity to the arterial wall. We assessed and quantified the extent of VSMC apoptosis on day 5 after pump implantation. The quantification of $TUNEL^+$ VSMCs in cerebral arteries suggested significantly reduced cell apoptosis in AAV-LH3-treated mice compared with that in AAV-GFP-treated mice (Figure 6(a)). Furthermore, the loss of VSMCs with decreased wall thickness was observed in AAV-GFP-treated small arteries (Figure 6(b)). In contrast, the cerebral arteries of the AAV-LH3-treated mice showed compensatory hypertrophy with wall thickening induced by hypertension (Figure 6(b), Supplemental Figure 11).

Discussion

In the present study, we investigated for the first time the effects of LH3 on the disease progression of ICH. We demonstrated that LH3 levels were reduced in human patients with ICH and were gradually decreased in mice before ICH. The incidence, number, and size of ICHs were markedly reduced in mice that received injections of AAV-LH3. AAV-LH3 treatment was sufficient to enhance BM integrity, inhibit MMP activity, attenuate microglial activation and leukocyte infiltration, and reduce VSMC apoptosis before ICH.

Despite the clinical importance of hypertensive ICH,[28] the cellular and molecular mechanisms that contribute to the pathogenesis of hypertensive ICH have not been well elucidated, and there are no effective treatments available for prevention.[29] Thus, ICH has a poor prognosis. Animal models of ICH are critical for studying the mechanisms and searching for possible targets for prevention and treatment. The most commonly used ICH models involve the injection of autologous blood or bacterial collagenase.[30] However, these models are mainly used for investigations of pathophysiology and potential therapeutic strategies of subsequent brain injury after ICH and may not be representative of what occurs in spontaneous human ICH. In this study, a model in which ICH was induced by s.c. AngII infusion and nitric oxide synthase inhibition (L-NAME) during chronic hypertension was used. This model is representative of the chronic and dynamic pathophysiological process that occurs before and after ICH and is useful for investigating mechanisms and intervention strategies to prevent the occurrence of ICH.[15,22]

LH3 is the only isoenzyme of LH that has the ability to glycosylate the hydroxylysine residues of collagen. LH3 is found in the lumen of the endoplasmic reticulum of cells but can be secreted into the extracellular space of tissues as well as into serum.[31] A recent study has revealed that LH3 is constitutively expressed in mouse tissues, such as lung, spleen, kidney and brain.[9] Additionally, immunofluorescence staining and immunoelectron microscopy have revealed that LH3 is mainly located in the BM and in the lumen of vessels. In our mouse ICH model, LH3 levels were reduced both in plasma and the cerebral vessels. Furthermore, a positive correlation existed between plasma LH3 levels and cerebral vessels, suggesting that plasma

LH3 levels may partially secreted from the cerebral vessels. In view of the combined data regarding the changes in LH3 levels in human patients with ICH and ICH mice, we speculate that LH3 found in human plasma may partially originate from the cerebral vessels, and the reduced LH3 levels in cerebral vessels of ICH patients may partially contribute to the reduction of LH3 levels in plasma. We must note that our human study was limited by the availability of only plasma samples, as patient brain tissue samples could not be used. Several studies have indicated that a reduction in LH3 causes deleterious changes to the deposition and organization of collagen and leads to human diseases, such as recessive dystrophic epidermolysis bullosa, which manifests as a significant reduction in LH3 and subsequent dermal-epidermal fragility in the skin of patients.[32] In agreement with previous studies, we found that LH3 levels were significantly decreased in human patients with ICH, suggesting the potential clinical significance of LH3 in ICH. Importantly, our results confirmed the gradually decreased levels of LH3 in cerebral vessels starting from the early stage (day 3) of hypertension prior to ICH in mice. Together with reduced collagen IV coverage, the disruption of BM integrity on day 5 and subsequent ICH, these results indicate that LH3 downregulation in cerebral vessels is a critical mechanism that participates in the pathophysiological process of ICH. Notably, despite the pivotal role of LH3 in ICH, the molecular mechanisms underlying LH3 downregulation under hypertension remain unclear and await further investigation.

Multiple lines of evidence suggest that hypertension is a major independent risk factor for ICH.[33,34] In the present study, treatment with AngII plus L-NAME resulted in comparable increases in blood pressure in both AAV-GFP- and AAV-LH3-treated mice. Notably, LH3 overexpression treatment did not further affect blood pressure, indicating that an antihypertension-independent mechanism was involved in the protective effects of AAV-LH3. By investigating the underlying mechanisms of the beneficial effects of AAV-LH3 treatment, our study became the first to provide transcriptional profiling data of cerebral vessels based on RNA-seq in a spontaneous ICH model. The expression dynamics of 62.8% of genes were significantly reversed by LH3 overexpression. Interestingly, genes modulated by LH3 were enriched in the collagen trimer and ECM, which belonged to the cellular component in the GO enrichment analysis. Our results are consistent with previous findings indicating that LH3 is essential for maintaining the deposition and organization of the ECM and for the formation of the BM.[31] The ECM of cerebral arterioles plays a pivotal role in preventing damaging overextension of the vascular wall, and the disruption and weakening of the ECM network are a critical factor in the development of ICH.[35] On the other hand, MMPs degrade collagen, laminin and other components of the BM, thereby compromising the structural integrity of the cerebral vessels. Previous studies have demonstrated that the activation of MMPs, especially MMP-2 and MMP-9, is involved in the weakening of the vessel wall in hypertensive ICH.[14,15] Consistent with these findings, our present data showed that MMP-9 and MMP-2 activities were increased after AngII and L-NAME treatment compared to the vehicle group. Furthermore, MMP-9 activity was significantly reduced after AAV-LH3 treatment. Together with the upregulation of collagen and laminin, these results support the notion that LH3 supplementation by AAV injection is sufficient to suppress the disruption and weakening of the ECM and maintain the integrity of the BM.

The transcriptional data in this study identified the involvement of several inflammation- and immune response-related pathways, such as the NF-kappa B and TNF signaling pathways, which was validated by microglial activation, adhesion molecule upregulation, leukocyte infiltration and proinflammatory cytokine production. This findings are in agreement with those of previous studies showing that hypertension induces P-selectin upregulation,[36] microglial activation and subsequent TNF-α release derived from microglia[37] in a spontaneous ICH model. Similarly, a pilot study based on RNA-seq demonstrated that different alternatively spliced genes from the whole blood of ICH patients were also involved in the cellular immune response.[38] We speculate that the inflammatory response may be secondary to the disrupted integrity of the BM and MMP activation and may lead to further ECM degradation and VSMC apoptosis in cerebral vessels.[39] VSMCs, mostly concentrated in the arteries and arterioles of the brain, are the predominant matrix-synthesizing cells and provide structural integrity to the vascular wall.[40] The mechanisms through which hypertension promotes the apoptosis of VSMCs in the cerebral vasculature mainly involve proinflammatory cytokines.[40] Recently, TNF-α was found to carry out proapoptotic actions in the VSMCs of cerebral aneurysms.[41] In line with this observation, our current study demonstrated increased levels of TNF-α and VSMC apoptosis in the small arteries of the brain under hypertension, followed by the thinning of the vascular wall. The loss of VSMCs may, in turn, lead to further impairments of collagen synthesis and deposition and ultimately cause vessel rupture.[42] Importantly, AAV-LH3 treatment dramatically reduced microglial activation, abolished the inflammatory process, attenuated VSMC apoptosis and ultimately prevented ICH.

In conclusion, we demonstrate that the overexpression of LH3 attenuates susceptibility to hypertension-induced spontaneous ICH. The protective effect of LH3 may involve its enhancement of BM integrity, suppression of inflammatory responses and reduction of VSMC apoptosis before ICH (a working model is depicted in Figure 6(c)). We emphasize that LH3 modulation may serve as a viable approach for future investigations of ICH prevention.

Funding

The author(s) disclosed receipt of the following financial support for the research, authorship, and/or publication of this article: The study was supported by the National Basic Research Program of China (2014CB541601 to JC), the CAMS Innovation Fund for Medical Sciences (CAMS-I2M, 2016-I2M-1-015 to JC), the National Natural Science Foundation of China (91539113 to JC, 81800263 to HL) and the Fundamental Research Funds for the Central Universities (3332018050 to HL).

Acknowledgments

We thank Kai Gao (the Institute of Laboratory Animal Science, CAMS & PUMC) for technical assistance with MRI.

Declaration of conflicting interests

The author(s) declared no potential conflicts of interest with respect to the research, authorship, and/or publication of this article.

Authors' contributions

HL and HX contributed to the experimental design, conducted experiments and data analysis and drafted the manuscript. HW, TL, YS and CB conducted experiments. JG, XW and LS collected human blood samples. YS, NX and YZ performed MRI experiments and contributed to manuscript preparation. JC participated in the experimental design, data analysis, and manuscript preparation.

Supplementary material

Supplementary material for this paper can be found at the journal website: http://journals.sagepub.com/home/jcb.

References

1. Wang W, Jiang B, Sun H, et al. Prevalence, incidence, and mortality of stroke in china: results from a nationwide population-based survey of 480–687 adults. *Circulation* 2017; 135: 759–771.
2. Feigin VL, Lawes CM, Bennett DA, et al. Worldwide stroke incidence and early case fatality reported in 56 population-based studies: a systematic review. *Lancet Neurol* 2009; 8: 355–369.
3. Metoki H, Ohkubo T, Kikuya M, et al. Prognostic significance for stroke of a morning pressor surge and a nocturnal blood pressure decline: the Ohasama study. *Hypertension* 2006; 47: 149–154.
4. Ungvari Z, Tarantini S, Kirkpatrick AC, et al. Cerebral microhemorrhages: mechanisms, consequences, and prevention. *Am J Physiol Heart Circ Physiol* 2017; 312: H1128–H1143.
5. Weng YC, Sonni A, Labelle-Dumais C, et al. COL4A1 mutations in patients with sporadic late-onset intracerebral hemorrhage. *Ann Neurol* 2012; 71: 470–477.
6. Jeanne M, Labelle-Dumais C, Jorgensen J, et al. COL4A2 mutations impair COL4A1 and COL4A2 secretion and cause hemorrhagic stroke. *Am J Hum Genet* 2012; 90: 91–101.
7. Jeanne M, Jorgensen J and Gould DB. Molecular and genetic analyses of collagen type IV mutant mouse models of spontaneous intracerebral hemorrhage identify mechanisms for stroke prevention. *Circulation* 2015; 131: 1555–1565.
8. Wang C, Risteli M, Heikkinen J, et al. Identification of amino acids important for the catalytic activity of the collagen glucosyltransferase associated with the multifunctional lysyl hydroxylase 3 (LH3). *J Biol Chem* 2002; 277: 18568–18573.
9. Salo AM, Wang C, Sipilä L, et al. Lysyl hydroxylase 3 (LH3) modifies proteins in the extracellular space, a novel mechanism for matrix remodeling. *J Cell Physiol* 2006; 207: 644–653.
10. Rautavuoma K, Takaluoma K, Sormunen R, et al. Premature aggregation of type IV collagen and early lethality in lysyl hydroxylase 3 null mice. *Proc Natl Acad Sci U S A* 2004; 101: 14120–14125.
11. Han MH, Kim JM, Yi HJ, et al. Predictors of supratentorial deep intracerebral hemorrhage volume and their effect on short-term mortality in Asians. *Cerebrovasc Dis* 2016; 42: 319–331.
12. Newman GC. Clarification of abc/2 rule for ICH volume. *Stroke* 2007; 38: 862.
13. Wang F, Han J, Higashimori H, et al. Long-term depression induced by endogenous cannabinoids produces neuroprotection via astroglial CB1R after stroke in rodents. *J Cereb Blood Flow Metab*. Epub ahead of print 12 February 2018. DOI: 10.1177/0271678X18755661.
14. Wakisaka Y, Chu Y, Miller JD, et al. Critical role for copper/zinc-superoxide dismutase in preventing spontaneous intracerebral hemorrhage during acute and chronic hypertension in mice. *Stroke* 2010; 414: 790–797.
15. Wakisaka Y, Chu Y, Miller JD, et al. Spontaneous intracerebral hemorrhage during acute and chronic hypertension in mice. *J Cereb Blood Flow Metab* 2010; 30: 56–69.
16. Ebert SN, Taylor DG, Nguyen HL, et al. Noninvasive tracking of cardiac embryonic stem cells in vivo using magnetic resonance imaging techniques. *Stem Cells* 2007; 25: 2936–2944.
17. Ni W, Mao S, Xi G, et al. Role of erythrocyte CD47 in intracerebral hematoma clearance. *Stroke* 2016; 47: 505–511.
18. Yamakawa H, Jezova M, Ando H, et al. Normalization of endothelial and inducible nitric oxide synthase expression in brain microvessels of spontaneously hypertensive rats by angiotensin II AT1 receptor inhibition. *J Cereb Blood Flow Metab* 2003; 23: 371–380.

19. Bengrine A, Da SC, Massy ZA, et al. Cerebral arterioles preparation and PECAM-1 expression in C57BL/6J and ApoE-/- mice. *Front Biosci* 2011; 16: 2367–2371.
20. Loinard C, Basatemur G, Masters L, et al. Deletion of chromosome 9p21 noncoding cardiovascular risk interval in mice alters Smad2 signaling and promotes vascular aneurysm. *Circ Cardiovasc Genet* 2014; 7: 799–805.
21. Xu H, Cao Y, Yang X, et al. ADAMTS13 controls vascular remodeling by modifying VWF reactivity during stroke recovery. *Blood* 2017; 130: 11–22.
22. Toth P, Tarantini S, Springo Z, et al. Aging exacerbates hypertension-induced cerebral microhemorrhages in mice: role of resveratrol treatment in vasoprotection. *Aging Cell* 2015; 14: 400–408.
23. Wang L, Fan W, Cai P, et al. Recombinant ADAMTS13 reduces tissue plasminogen activator-induced hemorrhage after stroke in mice. *Ann Neurol* 2013; 73: 189–198.
24. Ashino T, Yamamoto M and Numazawa S. Nrf2/Keap1 system regulates vascular smooth muscle cell apoptosis for vascular homeostasis: role in neointimal formation after vascular injury. *Sci Rep* 2016; 6: 26291.
25. Wu H, Wu T, Xu X, et al. Iron toxicity in mice with collagenase-induced intracerebral hemorrhage. *J Cereb Blood Flow Metab* 2011; 31: 1243–1250.
26. Han X, Zhao X, Lan X, et al. 20-HETE synthesis inhibition promotes cerebral protection after intracerebral hemorrhage without inhibiting angiogenesis. *J Cereb Blood Flow Metab*. Epub ahead of print 27 February 2018. DOI: 10.1177/0271678X18762645.
27. Wu CH, Shyue SK, Hung TH, et al. Genetic deletion or pharmacological inhibition of soluble epoxide hydrolase reduces brain damage and attenuates neuroinflammation after intracerebral hemorrhage. *J Neuroinflammation* 2017; 14: 230.
28. Walsh KB, Woo D, Sekar P, et al. Untreated hypertension: a powerful risk factor for lobar and nonlobar intracerebral hemorrhage in Whites, Blacks, and Hispanics. *Circulation* 2016; 134: 1444–1452.
29. Hemphill JC, Greenberg SM, Anderson CS, et al. Guidelines for the management of spontaneous intracerebral hemorrhage: a guideline for healthcare professionals from the American Heart Association/American Stroke Association. *Stroke* 2015; 46: 2032–2060.
30. MacLellan CL, Silasi G, Poon CC, et al. Intracerebral hemorrhage models in rat: comparing collagenase to blood infusion. *J Cereb Blood Flow Metab* 2008; 28: 516–525.
31. Risteli M, Ruotsalainen H, Salo AM, et al. Reduction of lysyl hydroxylase 3 causes deleterious changes in the deposition and organization of extracellular matrix. *J Biol Chem* 2009; 284: 28204–28211.
32. Watt SA, Dayal JH, Wright S, et al. Lysyl hydroxylase 3 localizes to epidermal basement membrane and is reduced in patients with recessive dystrophic epidermolysis bullosa. *PLoS One* 2015; 10: e0137639.
33. Romero JR, Preis SR, Beiser A, et al. Risk factors, stroke prevention treatments, and prevalence of cerebral microbleeds in the Framingham Heart Study. *Stroke* 2014; 45: 1492–1494.
34. Jeerakathil T, Wolf PA, Beiser A, et al. Cerebral microbleeds: prevalence and associations with cardiovascular risk factors in the Framingham Study. *Stroke* 2004; 35: 1831–1835.
35. Vanakker OM, Hemelsoet D and De Paepe A. Hereditary connective tissue diseases in young adult stroke: a comprehensive synthesis. *Stroke Res Treat* 2011; 2011: 712903.
36. Passos GF, Kilday K, Gillen DL, et al. Experimental hypertension increases spontaneous intracerebral hemorrhages in a mouse model of cerebral amyloidosis. *J Cereb Blood Flow Metab* 2016; 36: 399–404.
37. Meissner A, Minnerup J, Soria G, et al. Structural and functional brain alterations in a murine model of angiotensin II-induced hypertension. *J Neurochem* 2017; 140: 509–521.
38. Dykstra-Aiello C, Jickling GC, Ander BP, et al. Intracerebral hemorrhage and ischemic stroke of different etiologies have distinct alternatively spliced mRNA profiles in the blood: a pilot RNA-seq study. *Transl Stroke Res* 2015; 6: 284–289.
39. Moriwaki T, Takagi Y, Sadamasa N, et al. Impaired progression of cerebral aneurysms in interleukin-1beta-deficient mice. *Stroke* 2006; 37: 900–905.
40. Chalouhi N, Hoh BL and Hasan D. Review of cerebral aneurysm formation, growth, and rupture. *Stroke* 2013; 44: 3613–3622.
41. Jayaraman T, Berenstein V, Li X, et al. Tumor necrosis factor alpha is a key modulator of inflammation in cerebral aneurysms. *Neurosurgery* 2005; 57: 558–564.
42. Chalouhi N, Ali MS, Jabbour PM, et al. Biology of intracranial aneurysms: role of inflammation. *J Cereb Blood Flow Metab* 2012; 32: 1659–1676.